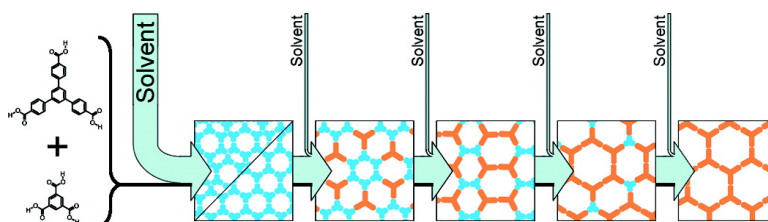


## Thermodynamical Equilibrium of Binary Supramolecular Networks at the Liquid#Solid Interface

Lorenz Kampschulte, Tova L. Werblowsky, Ravuri S. K. Kishore,  
 Michael Schmittl, Wolfgang M. Heckl, and Markus Lackinger

*J. Am. Chem. Soc.*, **2008**, 130 (26), 8502-8507 • DOI: 10.1021/ja801883t • Publication Date (Web): 06 June 2008

Downloaded from <http://pubs.acs.org> on February 8, 2009



### More About This Article

Additional resources and features associated with this article are available within the HTML version:

- Supporting Information
- Links to the 5 articles that cite this article, as of the time of this article download
- Access to high resolution figures
- Links to articles and content related to this article
- Copyright permission to reproduce figures and/or text from this article

[View the Full Text HTML](#)

## Thermodynamical Equilibrium of Binary Supramolecular Networks at the Liquid–Solid Interface

Lorenz Kampschulte,<sup>†,‡</sup> Tova L. Werblowsky,<sup>‡,⊥</sup> Ravuri S. K. Kishore,<sup>§</sup>  
Michael Schmittl,<sup>§</sup> Wolfgang M. Heckl,<sup>†,||</sup> and Markus Lackinger<sup>\*,†</sup>

*Department for Earth- and Environmental Sciences and Center for NanoScience (CeNS),  
Ludwig-Maximilians-University Munich, Theresienstrasse 41, D-80333 Munich, Germany,  
Department of Chemistry, Columbia University, New York, New York 10027, Center of Micro  
and Nanochemistry and Engineering, Organische Chemie I, Universität Siegen,  
Adolf-Reichwein-Strasse 2, D-57068 Siegen, Germany, and Deutsches Museum, Museumsinsel 1,  
D-80538 Munich, Germany*

Received March 13, 2008; E-mail: markus@lackinger.org

**Abstract:** Coadsorption of two different carboxylic acids, benzenetribenzoic acid and trimesic acid, was studied at the liquid–solid interface in two different solvents (heptanoic and nonanoic acid). Independent alteration of both concentrations in binary solutions resulted in six nondensely packed monolayer phases with different structures and stoichiometries, as revealed by means of scanning tunneling microscopy (STM). All of these structures are stabilized by intermolecular hydrogen bonding between the carboxylic acid functional groups. Moreover, phase transitions of the monolayer structures, accompanied by an alteration of the size and shape of cavity voids in the 2D molecular assembly, could be achieved by in situ dilution. The emergence of the various phases could be described by a simple thermodynamic model.

### Introduction

Two-dimensional supramolecular nanoporous networks of functionalized molecular components fabricated by self-assembly processes represent an interesting class of materials with promising potential for future technological impact.<sup>1–3</sup> Many applications, such as the arrangement of nanoscale objects (e.g., quantum dots) in regular arrays with a specific spacing, require highly structured surfaces. Today's lithographic production techniques<sup>4</sup> are far from being able to pattern surfaces with features in the low-nanometer regime. Self-assembly methods provide a promising, efficient, and reliable alternative approach for the rapid preparation of well-defined structures having nanoscale dimensions over a relatively large area.

A wide range of 2D ordered assemblies of organic molecules utilizing various noncovalent interactions such as hydrogen bonding,<sup>5–9</sup> dipolar coupling,<sup>10–12</sup> or metal coordination<sup>13</sup> has been investigated by means of submolecularly resolved STM

topographs. Hydrogen bonding in particular is a widely exploited mechanism for self-assembly of highly ordered monolayers, providing both high selectivity and directionality.<sup>14</sup>

While a large majority of networks are based on self-assembly of a single molecular component,<sup>15–17</sup> there has been growing interest in the design of multicomponent 2D assemblies.<sup>18–21</sup> However fabrication of a uniform multicomponent monolayer structure on a surface has been a challenging task. A number of binary mixtures investigated exhibit phase separation or irregular mixing.<sup>22–27</sup> Recently a few efforts have been successful in obtaining uniform monolayers of nanostructures from

<sup>†</sup> Ludwig-Maximilians-University Munich.

<sup>‡</sup> Columbia University.

<sup>§</sup> Universität Siegen.

<sup>||</sup> Deutsches Museum.

<sup>⊥</sup> Present address: Department of Chemistry and Physics, Touro College, 27-33 West 23 Street, New York, New York 10010.

- (1) Whitesides, G. M.; Mathias, J. P.; Seto, C. T. *Science* **1991**, *254*, 1312–1319.
- (2) Schickum, U.; Decker, R.; Klappenberger, F.; Zoppellaro, G.; Klyatskaya, S.; Ruben, M.; Silanes, I.; Arnau, A.; Kern, K.; Brune, H.; Barth, J. V. *Nano Lett.* **2007**, *7*, 3813–3817.
- (3) Furukawa, S.; Tahara, K.; De Schryver, F. C.; Van der Auweraer, M.; Tobe, Y.; De Feyter, S. *Angew. Chem., Int. Ed.* **2007**, *46*, 2831–2834.
- (4) Sheats, J. R.; Smith, B. W. *Microolithography Science and Technology*, 1st ed.; New York, 1998.
- (5) Chen, Q.; Frankel, D. J.; Richardson, N. V. *Langmuir* **2002**, *18*, 3219–3225.

- (6) Griessl, S.; Lackinger, M.; Edelwirth, M.; Hietschold, M.; Heckl, W. M. *Single Mol.* **2002**, *3*, 25–31.
- (7) Macdonald, J. C.; Whitesides, G. M. *Chem. Rev.* **1994**, *94*, 2383–2420.
- (8) Weckesser, J.; De Vita, A.; Barth, J. V.; Cai, C.; Kern, K. *Phys. Rev. Lett.* **2001**, *87*, 096101-1–4.
- (9) Keeling, D. L.; Oxtoby, N. S.; Wilson, C.; Humphry, M. J.; Champness, N. R.; Beton, P. H. *Nano Lett.* **2003**, *3*, 9–12.
- (10) Yokoyama, T.; Yokoyama, S.; Kamikado, T.; Okuno, Y.; Mashiko, S. *Nature* **2001**, *413*, 619–621.
- (11) de Wild, M.; Berner, S.; Suzuki, H.; Yanagi, H.; Schlettwein, D.; Ivan, S.; Baratoft, A.; Güntherodt, H. J.; Jung, T. A. *Chemphyschem* **2002**, *3*, 881–885.
- (12) Berner, S.; Brunner, M.; Ramoino, L.; Suzuki, H.; Güntherodt, H. J.; Jung, T. A. *Chem. Phys. Lett.* **2001**, *348*, 175–181.
- (13) Lin, N.; Dmitriev, A.; Weckesser, J.; Barth, J. V.; Kern, K. *Angew. Chem., Int. Ed.* **2002**, *41*, 4779–4783.
- (14) Jeffrey, G. A. *An Introduction to Hydrogen Bonding*. Oxford University Press: Oxford, 1997; Vol. 1, p 303.
- (15) Frommer, J. *Angew. Chem., Int. Ed.* **1992**, *31*, 1298–1328.
- (16) Cyr, D. M.; Venkataraman, B.; Flynn, G. W. *Chem. Mater.* **1996**, *8*, 1600–1615.
- (17) De Feyter, S.; De Schryver, F. C. *J. Phys. Chem. B* **2005**, *109*, 4290–4302.
- (18) Eichhorst-Gerner, K.; Stabel, A.; Moessner, G.; Declercq, D.; Valiyaveetil, S.; Enkelmann, V.; Müllen, K.; Rabe, J. P. *Angew. Chem., Int. Ed.* **1996**, *35*, 1492–1495.

multiple components leading to well defined patterns different from those of the individual components.<sup>28,29</sup> It is, however, desirable to have a tunable multicomponent 2D nanostructure whose cavity size and overall pattern could be modified, just by varying parameters such as the concentrations of the components.

In this work a two-dimensional self-assembled supramolecular system composed of two different carboxylic acids is studied. We present STM data for the different self-assembled structures and determine their area of stability in a two-dimensional phase diagram. A simple model is used to qualitatively explain the emergence of different structures in thermodynamical equilibrium with the liquid phase.

## Results and Discussion

Investigation of the subtle balance leading to coadsorption of two compounds, as well as the role of solvent identity, ready identification of the two species in STM images, and the possibility of preparing molecular mixtures in different solvents. Recent studies of relatively small molecules at the liquid–solid interface have demonstrated the stabilizing influence of hydrogen-bonds and the feasibility of fatty acids as solvents.<sup>30–34</sup> It has been shown, that carboxylic acid functional groups attached to an aromatic system drive the self-assembly process of monolayers on a graphite surface.<sup>35</sup>

Generally, predicting whether molecules will form mixed networks on a surface in equilibrium with a liquid phase is a quite difficult task. In the present study the similarity of symmetry and functional groups appear to promote the compatibility of BTB and TMA. In previous studies we combined 1,3,5-tris(4-pyridyl)-2,4,6-triazine (TPT) with TMA and terephthalic

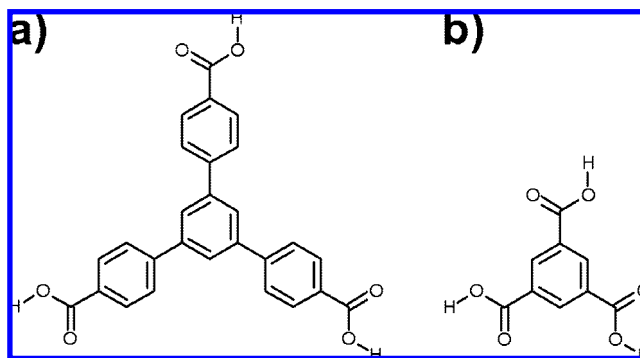


**Figure 1.** Structure of the adsorbates: (a) BTB (1,3,5-benzenetribenzoic acid) and (b) TMA (1,3,5-tricarboxybenzene, trimesic acid). Both molecules exhibit the same 3-fold symmetry ( $D_{3h}$ ) and have three carboxylic acid groups as intermolecular linkers attached to benzene rings.

acid.<sup>36</sup> However TPT does not have carboxylic acid groups (being both donor and acceptor for hydrogen bonds) and, therefore, requires a mediator to form stable monolayers at the liquid–solid interface near room temperature. BTB can be considered an enlarged derivative of TMA, with additional phenyl spacers between the carboxylic groups and the central benzene ring (cf. Figure 1). It has the ability to self-assemble in monolayers in different environments<sup>37,38</sup> and is considerably larger than TMA (diameter 1.8 vs 0.9 nm for TMA), thus easily distinguished in STM images. Since both molecules have carboxylic acid groups attached to a benzene ring, the homo- and heterointermolecular hydrogen bonds are very comparable, which is expected to facilitate cocrystallization.

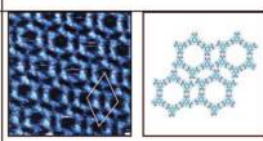
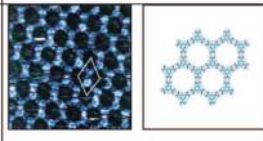
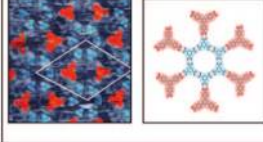
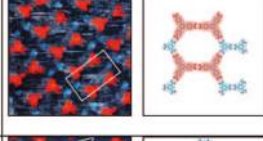
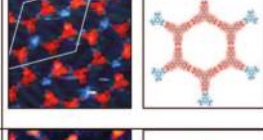
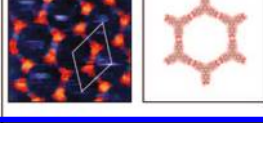
For the investigation of BTB + TMA coadsorption, two main parameters were changed: the ratio of BTB to TMA molecules in solution and the amount of solvent in the system (dilution). As solvents two alkanic acids with different chain lengths were used: heptanoic acid and nonanoic acid. The mixing ratio between the two unary saturated solutions (containing either BTB or TMA molecules) was varied between 2TMA + 1BTB (2 parts saturated solution of TMA and 1 part saturated solution of BTB) and 1TMA + 4BTB for the system with heptanoic acid as solvent and between 5TMA + 1BTB and 1TMA + 2BTB for the system with nonanoic acid. Diluted solutions were prepared by adding up to 10 parts solvent per part (mixed) saturated solution. From the mixing ratios, the relative concentrations of TMA (BTB) were calculated as the ratio of the volume portion containing TMA (BTB) to the total volume including the dilution with the other unary BTB (TMA) solution and pure solvent. Note that with this simple but reliable method of mixing saturated unary solutions only binary solutions with  $c_{\text{TMA}} + c_{\text{BTB}} \leq 100\%$  are accessible, where  $c_{\text{TMA}}$ ,  $c_{\text{BTB}}$  are the concentrations relative to a saturated solution ( $c_i = 100\%$ ).

In this two-dimensional concentration space six different self-assembled networks were observed: two networks consisting of only TMA molecules (A, B), one network containing only BTB molecules (F), and three mixed networks (C, D, E). Table 1

- (19) Qian, P.; Nanjo, H.; Yokoyama, T.; Suzuki, T. M. *Chem. Commun.* **1999**, 1197–1198.
- (20) Qian, P.; Nanjo, H.; Yokoyama, T.; Suzuki, T. M.; Akasaka, K.; Orhui, H. *Chem. Commun.* **2000**, 2021–2022.
- (21) Lei, S. B.; Wang, C.; Yin, S. X.; Bai, C. L. *J. Phys. Chem. B* **2001**, *105*, 12272–12277.
- (22) Venkataraman, B.; Breen, J. J.; Flynn, G. W. *J. Phys. Chem.* **1995**, *99*, 6608–6619.
- (23) Stevens, F.; Dyer, D. J.; Muller, U.; Walba, D. M. *Langmuir* **1996**, *12*, 5625–5629.
- (24) Hippius, K. W.; Lu, X.; Wang, X. D.; Mazur, U. *J. Phys. Chem. B* **1996**, *100*, 11207–11210.
- (25) Baker, R. T.; Mougous, J. D.; Brackley, A.; Patrick, D. L. *Langmuir* **1999**, *15*, 4884–4891.
- (26) Padowitz, D. F.; Sada, D. M.; Kemer, E. L.; Dougan, M. L.; Xue, W. A. *J. Phys. Chem. B* **2002**, *106*, 593–598.
- (27) De Feyter, S.; Larsson, M.; Schuurmans, N.; Verkuijl, B.; Zorinants, G.; Gesquiere, A.; Abdel-Mottaleb, M. M.; van Esch, J.; Feringa, B. L.; van Stam, J.; De Schryver, F. C. *Chem. Eur. J.* **2003**, *9*, 1198–1206.
- (28) De Feyter, S.; Miura, A.; Yao, S.; Chen, Z.; Wurthner, F.; Jonkheijm, P.; Schenning, A. P. H. J.; Meijer, E. W.; De Schryver, F. C. *Nano Lett.* **2005**, *5*, 77–81.
- (29) Yang, X. Y.; Mu, Z. C.; Wang, Z. Q.; Zhang, X.; Wang, J.; Wang, Y. *Langmuir* **2005**, *21*, 7225–7229.
- (30) Griessl, S. J. H.; Lackinger, M.; Jamitzky, F.; Markert, T.; Hietschold, M.; Heckl, W. M. *J. Phys. Chem. B* **2004**, *108*, 11556–11560.
- (31) Hietschold, M.; Lackinger, M.; Griessl, S.; Heckl, W. M.; Gopakumar, T. G.; Flynn, G. W. *Microelectron. Eng.* **2005**, *82*, 207–214.
- (32) De Feyter, S.; De Schryver, F. C. *Chem. Soc. Rev.* **2003**, *32*, 139–150.
- (33) Yan, H.-J.; Lu, J.; Wan, L.-J.; Bai, C.-L. *J. Phys. Chem. B* **2004**, *38*, 11251–11255.
- (34) Lei, S. B.; Wang, C.; Yin, S. X.; Wang, H. N.; Xi, F.; Liu, H. W.; Xu, B.; Wan, L. J.; Bai, C. L. *J. Phys. Chem. B* **2001**, *105*, 10838–10841.
- (35) Lu, J.; Zeng, Q.-d.; Wang, C.; Zheng, Q.-y.; Wana, L.; Bai, C. J. *Mater. Chem.* **2002**, *12*, 2856–2858.

- (36) Kampschulte, L.; Griessl, S.; Heckl, W. M.; Lackinger, M. *J. Phys. Chem. B* **2005**, *109*, 14074–14078.
- (37) Kampschulte, L.; Lackinger, M.; Maier, A. K.; Kishore, R. S. K.; Griessl, S.; Schmittel, M.; Heckl, W. M. *J. Phys. Chem. B* **2006**, *110*, 10829–10836.
- (38) Ruben, M.; Payer, D.; Landa, A.; Comisso, A.; Gattinoni, C.; Lin, N.; Collin, J. P.; Sauvage, J. P.; De Vita, A.; Kern, K. *J. Am. Chem. Soc.* **2006**, *128*, 15644–15651.
- (39) Florio, G. M.; Werblowsky, T. L.; Müller, T.; Berne, B. J.; Flynn, G. W. *J. Phys. Chem. B* **2005**, *109*, 4520–4532.

**Table 1.** Observed Two-Dimensional Structures for the BTB–TMA System<sup>a</sup>

|   |  | unit cell parameters                                 | area density [1/nm <sup>2</sup> ]                            | relative coverage [%]   |
|---|--|--|--|---|
| A |   | a = b = 2.5 nm<br>$\alpha = 120^\circ$               | $\sigma_{\text{BTB}} = 0.00$<br>$\sigma_{\text{TMA}} = 1.11$ | $\rho_{\text{BTB}} = 0.0$<br>$\rho_{\text{TMA}} = 84$<br>$\rho_{\text{cavity}}(\text{exp}) = 16$<br>$\rho_{\text{cavity}}(\text{sim}) = 16$ |
| B |   | a = b = 1.7 nm<br>$\alpha = 120^\circ$               | $\sigma_{\text{BTB}} = 0.00$<br>$\sigma_{\text{TMA}} = 0.80$ | $\rho_{\text{BTB}} = 0.0$<br>$\rho_{\text{TMA}} = 61$<br>$\rho_{\text{cavity}}(\text{exp}) = 39$<br>$\rho_{\text{cavity}}(\text{sim}) = 37$ |
| C |   | a = b = 4.3 nm<br>$\alpha = 120^\circ$               | $\sigma_{\text{BTB}} = 0.13$<br>$\sigma_{\text{TMA}} = 0.39$ | $\rho_{\text{BTB}} = 22$<br>$\rho_{\text{TMA}} = 29$<br>$\rho_{\text{cavity}}(\text{exp}) = 49$<br>$\rho_{\text{cavity}}(\text{sim}) = 51$  |
| D |   | a = 4.3 nm<br>b = 2.5 nm<br>$\alpha = 90^\circ$      | $\sigma_{\text{BTB}} = 0.19$<br>$\sigma_{\text{TMA}} = 0.19$ | $\rho_{\text{BTB}} = 32$<br>$\rho_{\text{TMA}} = 14$<br>$\rho_{\text{cavity}}(\text{exp}) = 54$<br>$\rho_{\text{cavity}}(\text{sim}) = 54$  |
| E |   | a = b = 5.7 nm<br>b = 5.7 nm<br>$\alpha = 120^\circ$ | $\sigma_{\text{BTB}} = 0.21$<br>$\sigma_{\text{TMA}} = 0.07$ | $\rho_{\text{BTB}} = 36$<br>$\rho_{\text{TMA}} = 5.0$<br>$\rho_{\text{cavity}}(\text{exp}) = 59$<br>$\rho_{\text{cavity}}(\text{sim}) = 54$ |
| F |  | a = b = 3.2 nm<br>$\alpha = 120^\circ$               | $\sigma_{\text{BTB}} = 0.23$<br>$\sigma_{\text{TMA}} = 0.00$ | $\rho_{\text{BTB}} = 38$<br>$\rho_{\text{TMA}} = 0.0$<br>$\rho_{\text{cavity}}(\text{exp}) = 62$<br>$\rho_{\text{cavity}}(\text{sim}) = 53$ |

<sup>a</sup> On the left hand side STM-images of the different structures are shown, where TMA molecules are colored blue, and the larger triangular-shaped BTB molecules are colored orange (image size  $10 \times 10 \text{ nm}^2$ ). Molecular mechanics simulations (frame size  $7.5 \times 7.5 \text{ nm}^2$ ) are depicted right next to the STM-images. Errors for the experimentally determined unit cell parameters:  $\Delta a = \Delta b = \pm 0.15 \text{ nm}$ ,  $\Delta \alpha = \pm 3^\circ$ . Area densities ( $\sigma_{\text{BTB}}$ ,  $\sigma_{\text{TMA}}$ ) and the relative surface coverage of molecules ( $\rho_{\text{BTB}}$ ,  $\rho_{\text{TMA}}$ ) and cavities ( $\rho_{\text{cavity}}(\text{exp})$ ) were calculated from experimental unit cell parameters;  $\rho_{\text{cavity}}(\text{sim})$  denotes the slightly adjusted values as used to simulate the phase diagram.

summarizes the experimentally determined lattice parameters for all observed structures. The relative area densities of BTB and TMA respectively were estimated by applying the projected area of the van der Waals surface of flat lying molecules. This results in an area of  $1.69 \text{ nm}^2$  for one BTB and  $0.76 \text{ nm}^2$  for one TMA molecule including the area occupied by intermolecular bonds. The remaining area was taken as the cavity size on the surface. Structures A and B are well-known from previous experiments with TMA on graphite, both in UHV<sup>6</sup> and at the liquid–solid interface.<sup>31</sup> By applying a homologous series of fatty acids as solvents, we have shown that the formation of two TMA polymorphs at the liquid–solid interface can be controlled by solvent identity. In the case of heptanoic acid the growth of both the so-called “flower” (A) and the “chickenwire” (B) TMA polymorphs was revealed, occasionally in coexistence. Solvents with a longer aliphatic tail, e.g. nonanoic acid, precipitate exclusively structure B. The structures C, D, and E are mixed networks, comprising both BTB and TMA molecules in different stoichiometries. Structure C consists of six-

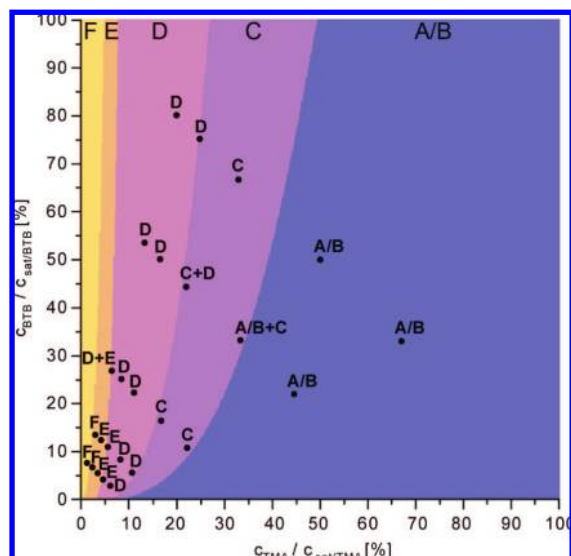


**Figure 2.** Phase diagram of the bimolecular system TMA + BTB in heptanoic acid. The abscissa depicts the relative TMA-concentration, the ordinate depicts the relative BTB-concentration. Both concentrations are normalized to the concentration of saturated unary solutions, i.e., the solubility of the respective compound. Experimentally probed points and observed structures are indicated in the diagram. Uniformly colored regions depict the area of stability of the different structures (assignment on top), resulting from the thermodynamic model.

membered TMA rings, with three of these rings being interconnected by one BTB molecule. Both TMA–TMA and BTB–TMA bonds are 2-fold hydrogen bonds between adjacent carboxylic groups. The directionality and reversibility of the hydrogen bonds is clearly an important factor that determines the formation and stability of these structures. All networks, except for structure A, exhibit the energetically most favorable hydrogen-bonding angle of  $180^\circ$  for the carboxylic acid dimers. E is the inverse structure of C, thus it is built up of six-membered BTB rings interconnected by TMA molecules. It can be constructed from C by interchanging TMA and BTB molecules. Except for structure D all observed networks can be described by a hexagonal unit cell. The unit cell of structure D is rectangular and contains an equal number of TMA and BTB molecules. Structure F is the corresponding network to B, but with BTB molecules instead of TMA and therefore an enlarged lattice constant and cavity size. This structure was found previously for unary BTB solutions.<sup>37</sup> However, in this study the BTB chickenwire network was exclusively observed with nonanoic acid as solvent. For heptanoic acid a rectangular network was found. Apparently, when TMA is present in small concentrations, playing the role of an impurity, it can influence the self-assembly of BTB monolayers.

Figure 2 depicts the phase diagram of the concentration-space probed with heptanoic acid as solvent. The structures containing predominantly TMA molecules were observed on the right-hand side, that is, for solutions with high TMA concentration, whereas networks mainly build up of BTB molecules occur on the left-hand side, implying a very low TMA concentration.

In the following a thermodynamic equilibrium model is applied to qualitatively explain the structural versatility of the binary TMA + BTB system. This approach is based on the monotonic increase of the chemical potential of the respective compound with concentration. In this model the Gibbs free energy  $G$  of each structure is calculated under the assumption of thermodynamic equilibrium, that is,  $\partial \Delta G = 0$  or equality of the chemical

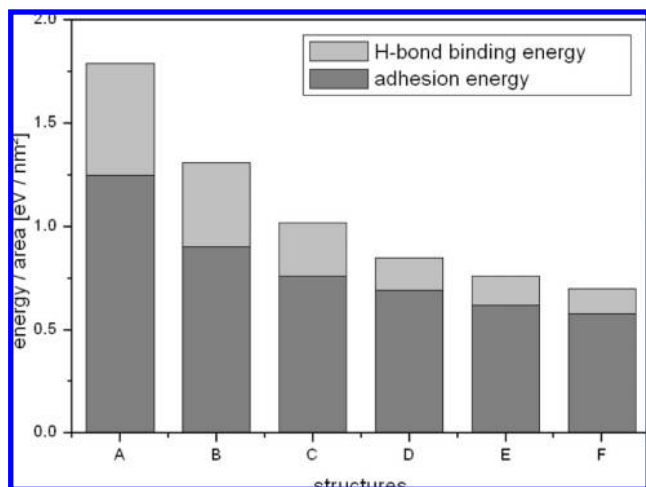


**Figure 3.** Molecular mechanics calculations: total binding energies of the different observed structures, split into adhesion energy between the molecules and the surface and the intermolecular H-bond binding energy. For better comparability, the respective energies have been normalized to the surface area.

potentials  $\mu_{\text{TMA}}$  and  $\mu_{\text{BTB}}$  of both TMA and BTB on the surface and in solution. The Gibbs free energy of each structure is then given by

$$G = [\sigma_{\text{TMA}}(\text{structure})\mu_{\text{TMA}}(c_{\text{TMA}}) + \sigma_{\text{BTB}}(\text{structure})\mu_{\text{BTB}}(c_{\text{BTB}}) + e_{\text{solvent}}\rho_{\text{cavity}}(\text{structure})]A \quad (1)$$

Here  $\sigma(\text{structure})$  denotes the area densities (molecules/unit area) of TMA and BTB for the respective structure, the index (structure) runs from A to F. The last term includes solvent coadsorption within the cavities as discussed in more detail below, where  $e_{\text{solvent}}$  denotes the additional free energy per unit area associated with the adsorption of solvent molecules within the cavity and  $\rho_{\text{cavity}}(\text{structure})$  the relative cavity area portion of the respective structure. All structure dependent values are summarized in Table 1.

This model assumes that the chemical potential of the adsorbates is a function of concentration but remains virtually constant during monolayer growth. Since the number of molecules needed to form the monolayer is about 2 orders of magnitude smaller than the quantity in the liquid phase, the concentration, and hence the chemical potential of each species in solution, can be assumed constant.

A molecular mechanics simulation was performed to calculate the binding energies of the different structures (for methodical details see ref 39). For these calculations the experimental unit cell parameters were employed as a constraint. Figure 3 shows the total binding energy of the various structures and the relative fractions resulting from H-bonding and adhesion of the aromatic systems to the graphite surface. As expected, the adhesion energy of the monolayer is exactly proportional to the relative area covered by TMA and BTB, and, thus, to the area of interaction between the aromatic  $\pi$ -systems of the molecules and the electron system of the graphite substrate.

Although molecular mechanics simulations neglect and approximate a number of interactions in such a system which are important for determining the absolute value of the binding energy, they allow a relative comparison to be made among different monolayer surface structures. Since all structures employ the same substrate and have the same bond type and the same molecules in common, considerable insight into the

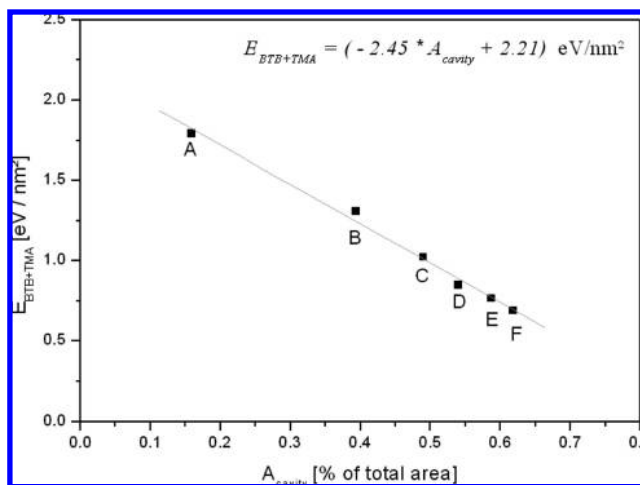


**Figure 4.** Plot of the calculated monolayer stabilization energy  $E_{\text{BTB+TMA}}$  versus cavity area  $A_{\text{cavity}}$ . Capital letters A–F indicate the structure associated with each data point. Values for the adhesion + intermolecular bonding energy of the BTB + TMA networks were taken from the molecular mechanics simulations, whereas  $A_{\text{cavity}}$  was calculated in the way described in the text body from the experimental unit cell parameters. The dotted line represents a linear fit.

relative energetics can be obtained even from such simplified model calculations. As is evident from Table 1, the cavity area portion increases monotonically from structure D to F, whereas both the adhesion and H-bonding energies of the molecules decrease monotonically. A plot of the binding energy as calculated by molecular mechanics simulations versus the cavity area of structures A to F is depicted in Figure 4. It is obvious that the larger the cavity area is, the smaller is the adsorption energy from the BTB and TMA monolayer structure. The dotted line represents a linear fit with a regression coefficient of  $r^2 = 0.99$ . Generally, in a polymorphic system the total free energy of all phases is comparable within the scale of thermal energy.<sup>40</sup> Here the molecular mechanics simulations of the adsorbed monolayer indicate that the adhesion plus H-bonding energies differ by about a factor of 2 over the range of systems studied. However, these calculations neglect the role of solvent coadsorption within the cavities where pristine substrate is exposed to solution. To account for further contributions to the stabilization energy of the monolayer through solvent coadsorption the additional term  $e_{\text{solvent}}$  times  $\rho_{\text{cavity}}(\text{structure})$  in eq 1 was introduced. Thus the cavity contribution to the total free energy was assumed to be proportional to the cavity area with a universal, that is, structure independent energy density  $e_{\text{solvent}}$ . Of course, this rather crude continuum model neglects the fact that a discrete number of solvent molecules adsorbs within the cavities and that they might differ in their adsorption geometry and energy depending on the cavity size and shape. The hypothesis of cavity occupation by solvent molecules is supported by observation of various types of image contrast within the cavities (cf. Supporting Information).

Based on eq 1 the phase diagram for BTB + TMA monolayer structures was simulated in the following way. For each point in concentration space ( $c_{\text{TMA}}$ ,  $c_{\text{BTB}}$ ) the chemical potential of TMA and BTB respectively was evaluated based on the concentration dependence of a regular solution:

$$\mu_i(c_i) = \mu_{0,i} + \varepsilon(1 - c_i)^2 + kT \ln c_i \quad (2)$$

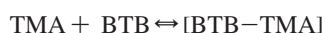
(40) Gavezzotti, A. *Crystengcomm.* **2002**, 343–347.

where index  $i$  refers to the compound, that is, TMA or BTB,  $c_i$  stands for the concentration, and  $k$ , and  $T$  are Boltzmann constant and temperature. The first term  $\mu_{0,i}$  is the standard chemical potential of the respective compound, the second term accounts for the enthalpy of mixing, and the third term stands for the entropy of mixing. Since the interaction of both TMA and BTB with the solvent is expected to be similar, a universal value for  $\epsilon$  was used.

The values of  $\mu_{\text{TMA}}$  and  $\mu_{\text{BTB}}$  at the point ( $c_{\text{TMA}}$ ,  $c_{\text{BTB}}$ ) were used to evaluate the total free energy  $G$  of the monolayer according to eq 1 for all structures A–F, applying the area densities of BTB, TMA, and the cavity area of the respective structure. Finally this specific point in the two-dimensional concentration space was assigned to the structure exhibiting the minimum in free energy. Starting from an initial guess for the free parameters ( $\mu_{0\text{TMA}}$ ,  $\mu_{0\text{BTB}}$ ,  $\epsilon$ ,  $e_{\text{solvent}}$ ), iterations were performed until the visually best fit was obtained. Simulations were performed for a quadratic grid ( $\Delta c_i = 0.1\%$ ) of TMA and BTB concentrations, the result is underlaid in Figure 2. To exactly reproduce the experimental phase diagram, the cavity area portions of the structures were slightly adjusted. The modified values as used for the simulation are also stated in Table 1. It is noteworthy, that the order of the phases in the simulated phase diagram is very robust with respect to other functions for the concentration dependence of the chemical potential and the fit parameters. Only the exact location of the phase boundaries and the stability of distinct phases depend on the adjustable parameters. Furthermore, in regions where structures A/B represent the thermodynamically most stable phase (this is the right-hand side of the phase diagram), structure B leads to the minimum in  $G$  due to its larger cavity area and the affiliated solvent coadsorption. However, the stabilization of phase A might be caused by kinetic effects as elaborately discussed in previous work.<sup>31</sup> In addition, the area of stability for coexistence of two phases in the vicinity of the respective phase boundary was investigated (see Supporting Information for details). In agreement with the experimental finding that phase coexistence is rarely observed the model predicts rather narrow regions in concentration space where two phases are thermodynamically stable. This indicates that the energetic difference between the distinct phases is still substantial which results in sharp transitions as a function of concentration. Gradual transitions where extended concentration regions exhibit phase coexistence can only be observed when the energetic difference between the respective phases is small.<sup>41</sup>

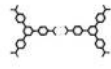
One possible explanation for the observation of multiple arrangements of BTB and TMA on the surface is the formation of basic supramolecular units. Relevant building blocks comprise  $[\text{TMA}]_2$ ,  $[\text{BTB}]_2$ ,  $[\text{BTB-TMA}]$ , or  $[\text{TMA}]_3$ . As depicted in Table 2 all networks can be built up from these basic units.

Of course, all structures could be seeded by even larger supramolecular units; however, their stability in solution is likely to be low. Encounters of two monomers in solution or on the substrate result in formation of supramolecular dimers:



At constant temperature formation and decay rates determine the equilibrium between monomers and dimers. For example, as the BTB concentration is increased, the formation of mixed

**Table 2.** Decomposition of the Six Different Network Structures into Four Distinct Supramolecular Building Blocks<sup>a</sup>

| structure | $[\text{TMA}]_3$  | $[\text{TMA}]_2$  | $[\text{TMA-BTB}]$  | $[\text{BTB}]_2$  |
|-----------|---|---|---|---|
|           |  |  |  |  |
| A         | 100%  |   |   |   |
| B         |   | 100%  |   |   |
| C         |   | 50%   | 50%   |   |
| D         |   | 50%   |   | 50%   |
| E         |   |   | 50%   | 50%   |
| F         |   |   |   | 100%  |

<sup>a</sup> The numbers indicate the proportion of the respective dimer or trimer.

$[\text{BTB-TMA}]$  and eventually  $[\text{BTB}]_2$  dimers becomes favored based on the law of mass action. As the concentration of supramolecular units in solution increases, the possibility of seeding the different structures A–F on the surface will be enhanced. Since the surface structures are in dynamic equilibrium with the liquid phase, altering the stability of the various basic supramolecular units in solution will change the surface structure as well.

For the experiments using nonanoic acid as a solvent, similar network structures were found. The arrangement of the structures in the phase diagram is similar to that for heptanoic acid as a solvent. For saturated solutions containing a high concentration of TMA molecules, networks consisting only of TMA molecules were observed. In accordance with previous results,<sup>31</sup> only structure B and not A was observed using nonanoic acid as solvent. For mixtures with higher BTB concentration and higher dilution, structure F, the pure BTB chickenwire network, was found. The mixed structure E was found in the regime between these two extreme cases.

All experiments described so far were conducted with premixed binary solutions, but it is of interest to evaluate whether anticipated phase transitions can also be induced by in situ dilution. To test this idea, a droplet ( $\sim 5 \mu\text{L}$ ) of premixed binary solution was applied to the graphite sample, and the emerging monolayer was imaged with the STM. Then the tip was retracted, a small amount of solvent ( $\sim 1 \mu\text{L}$ ) was added to the sample, the tip was reapproached immediately, and the modified system was imaged. Dilution was repeated in a stepwise manner until all network structures were eventually dissolved. Although the concentration after dilution is not precisely defined, each single phase along the dilution-path in the phase diagram could be addressed. Because adding solvent dilutes both BTB and TMA equally, the dilution-path is a straight line from the initial set of concentrations toward the origin of the phase diagram.

These experiments were carried out with different starting solutions. For instance, beginning with structure B at  $c_{\text{TMA}} = c_{\text{BTB}} = 50\%$ , stepwise diluting results in phases C, D and eventually E. Upon further dilution TMA/BTB monolayers were no longer observable. The time scale for the phase transitions at room temperature is less than 30 s, which is the minimum time needed to reapproach the STM tip and restart the scanning process after deposition of additional solvent. Generally, it was possible to induce phase transitions between different networks and, therefore, to change the size of the surface monolayer

(41) Lei, S.; Tahara, K.; De Schryver, F. C.; Van der Auweraer, M.; Tobe, Y.; De Feyter, S. *Angew. Chem., Int. Ed.* **2008**, *47*, 2964–2968.

cavities directly (in situ) by just adding solvent. Furthermore, the structural changes initiated by varying the concentrations of the binary supernatant solution unambiguously prove that the adsorbed monolayers are in thermodynamical equilibrium with the liquid phase.

## Conclusions

The phase diagram of a binary system was probed at the liquid–solid interface by means of in situ STM. Depending on the concentrations of the two solutes, TMA and BTB, six different hydrogen-bonded monolayer structures were observed, three of these being mixed TMA+BTB phases. Although both species are always present in solution, the different molecular arrangements on the surface range from pure TMA networks to different hexagonal and rectangular mixed networks (containing BTB and TMA) to arrangements built up from just BTB molecules. All networks exhibit a periodic arrangement of large internal cavities of various sizes (1.1–2.8 nm) and shapes. The cavities are potential sites for the templated adsorption of appropriate guests within the host networks. When using the slightly different molecule nonanoic acid as a solvent, similar network surface structures were found. Probing the two-dimensional TMA + BTB concentration space with premixed solutions allowed the construction of a phase diagram of the system. In addition, in situ dilution of the samples with pure solvent initiated phase transitions as anticipated from and consistent with the phase diagram, thereby proving that the growth of these mixed networks is thermodynamically controlled. The switchability of these networks provides an opportunity to construct monolayer host networks that offer a tunable cavity size, lattice parameters, and composition.

The measured phase diagram was reproduced by means of a simple thermodynamic model, based on the concentration

dependence of the chemical potential for TMA and BTB in solution. Measured unit cell parameters of the respective structures and the related molecular area densities of the two compounds were employed as experimental input to this simulation.

The incorporation of other molecules in the BTB + TMA template structure could be used to introduce long-range order among the guest species or immobilize them, for example, for local spectroscopy. The remarkably rich phase diagram of this binary system makes six different surface structures readily accessible by simply varying the concentration of just two compounds.

**Acknowledgment.** We are particularly grateful to George W. Flynn and Bruce J. Berne for their essential and encouraging support. This work was funded by the National Science Foundation under Grant CHE-03-52582 and by the Nanoscale Science and Engineering Initiative of the National Science Foundation under NSF Award Number CHE-01-17752 and by the New York State Office of Science, Technology, and Academic Research (NYSTAR). We thank the cluster of excellence “Nanosystems Initiative Munich” (NIM) and the SFB 486 for valuable support. L.K. thanks the German Academic Exchange Service (DAAD) for fellowship support, which made this research possible.

**Supporting Information Available:** Experimental procedures and experimental evidence for coadsorption of solvent molecules within the cavities; extended version of the thermodynamic model including mixed phases. This material is available free of charge via the Internet at <http://pubs.acs.org>.

JA801883T